



Frontiers of synchrotron research in materials science

Klaus-Dieter Liss and Kai Chen, Guest Editors

Synchrotron radiation has evolved tremendously in recent decades in sources, instrumentation, and applications in materials studies. This article provides background and an introduction to the state of the art of synchrotron research as it relates to materials research, including an overview of the articles in this *MRS Bulletin* issue, which focus on Laue microdiffraction, high-energy x-ray diffraction on battery materials, synchrotron radiation in high-pressure research, x-ray dark-field microscopy, and x-ray absorption spectroscopy applied to energy research. The modern approach of displaying diffraction data in reciprocal-space units and the distinction between spectroscopy and diffraction are summarized. Applications and technologies are continuously developing toward technical and optical limits, combining multiple methods for an even brighter future for this field. It is now time for expert groups to begin applying multiple and different kinds of quantum beams, such as neutrons, muons, electrons, and ions, complementary to synchrotron radiation for more efficient and effective characterization of materials.

Introduction

Since the early days (beginning in 1956), when x-rays were extracted as a byproduct in circular electron and positron accelerators,¹ synchrotron radiation has developed tremendously, with brilliances (photons/s/mm²/mrad²/[0.1% bandwidth]) increasing faster than the often-cited Moore's Law of computer-memory capacity. In so-called storage rings, electrons or positrons circulate and emit synchrotron radiation (see **Figure 1**). Subsequent to its parasitic use at high-energy particle-physics laboratories, rings were refurbished for the delivery of synchrotron radiation (second generation). For the third generation, dedicated facilities were optimally designed and newly built. Three third-generation high-energy storage rings for synchrotron radiation have been built and continuously refurbished since the 1990s, namely the European Synchrotron Radiation Facility (ESRF, 1994), the Advanced Photon Source (APS, 1996), and Super Photon Ring-8 GeV (SPring-8, 1997) (see **Figure 2**), followed in the past decade by Deutsche Elektronen Synchrotron DESY's PETRA-III (former Positron-Elektron-Tandem-Ring-Anlage) (2009). Their high-particle energies of 6 GeV, 7 GeV, 8 GeV, and 6 GeV, respectively, allow for undulator radiation into the high-energy x-ray range (100 keV) necessary for bulk studies in materials science and engineering, as well as other advantages, such as easy penetration into sample

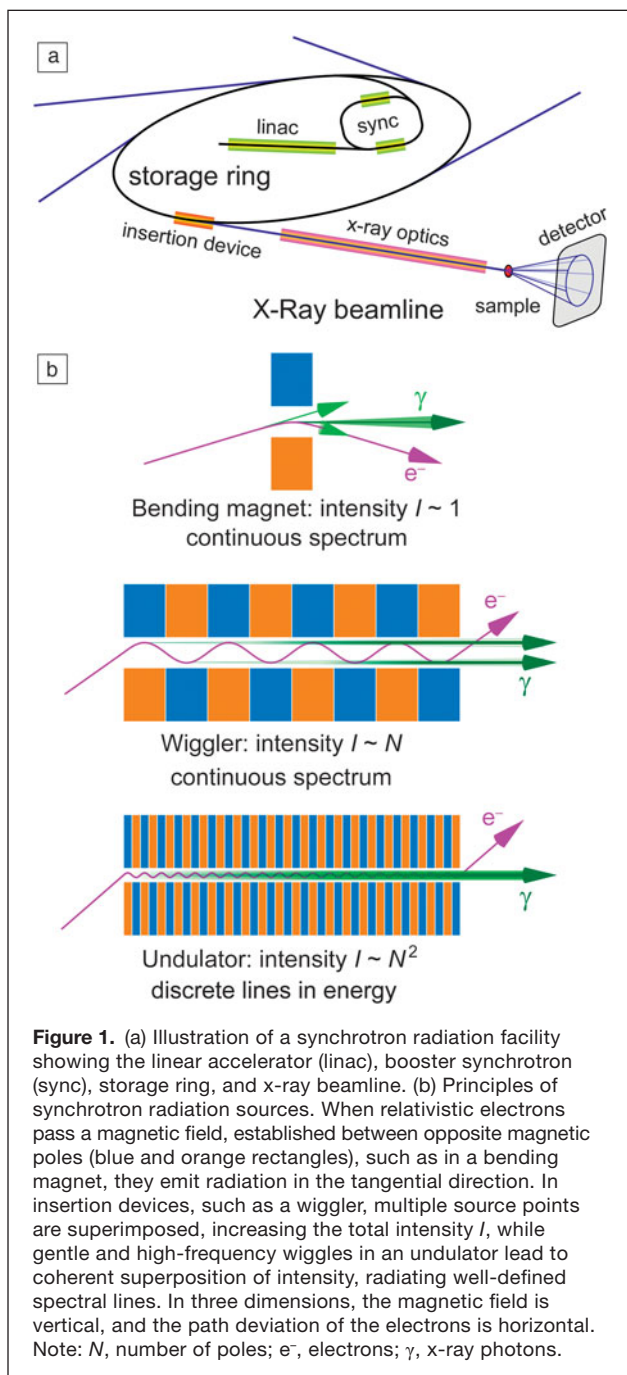
environments, small scattering angles, and large reciprocal-space coverage.²

Numerous 3 GeV storage rings have been established all over the world, including the Diamond Light Source, Canadian Light Source, Taiwan National Synchrotron Radiation Research Center, Swiss Light Source, Australian Synchrotron, Shanghai Synchrotron Radiation Facility, Pohang Light Source, and National Synchrotron Light Source II. The flagships of such medium-energy rings have been trimmed to ultimate, diffraction-limited brightness in the soft (0.1 to 1 keV) to hard x-ray range (10 keV), delivering brilliance and a high degree of coherent light. A multitude of applications for all ranges of x-rays have evolved, including dedicated niches, such as absorption spectroscopy, inelastic scattering, surface scattering, and deep-bulk diffraction, which is beyond the scope of this article. This multitude also implies the necessity and existence of different-purpose storage rings (i.e., synchrotrons), varying in size and energy by orders of magnitude. Comprehensive information on facilities, techniques, applications, and news can be found on the LightSources.org website.³

This article discusses the underpinning concepts of diffraction, spectroscopy, and imaging, and traces the use of various x-ray energy ranges applicable to the contributions in this issue of *MRS Bulletin*.

Klaus-Dieter Liss, Australian Nuclear Science and Technology Organisation, Australia; and School of Mechanical, Materials & Mechatronic Engineering, University of Wollongong, Australia; kdl@ansto.gov.au

Kai Chen, Center for Advancing Materials Performance from the Nanoscale, State Key Laboratory for Mechanical Behavior of Materials, Xi'an Jiaotong University, China; kchenlb@gmail.com
doi:10.1557/mrs.2016.112



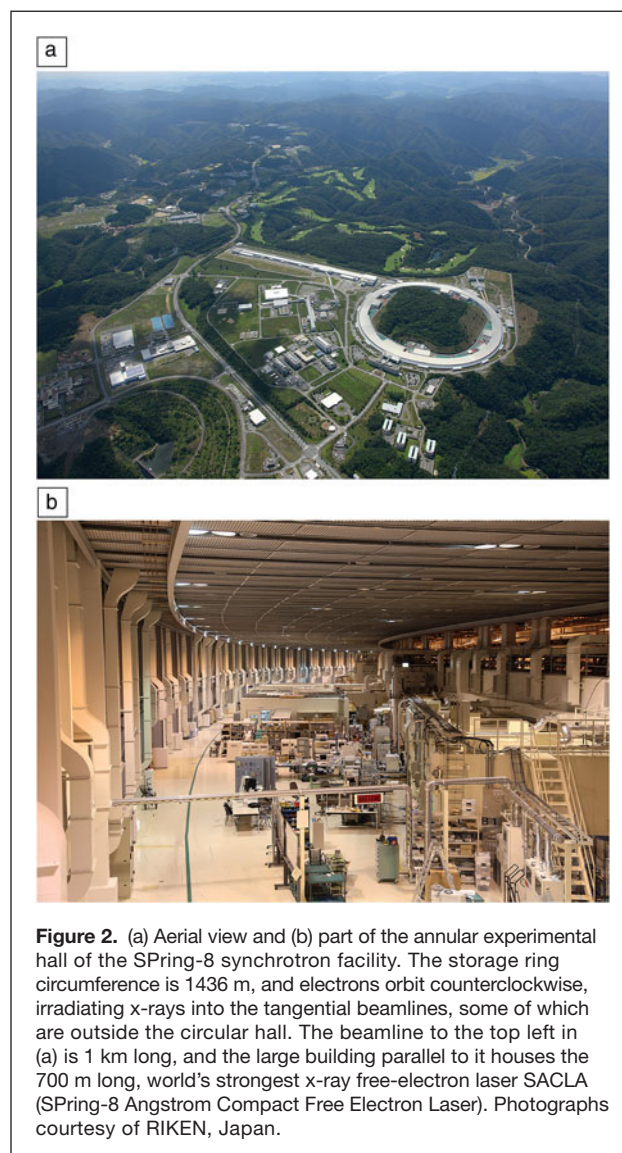
X-ray techniques

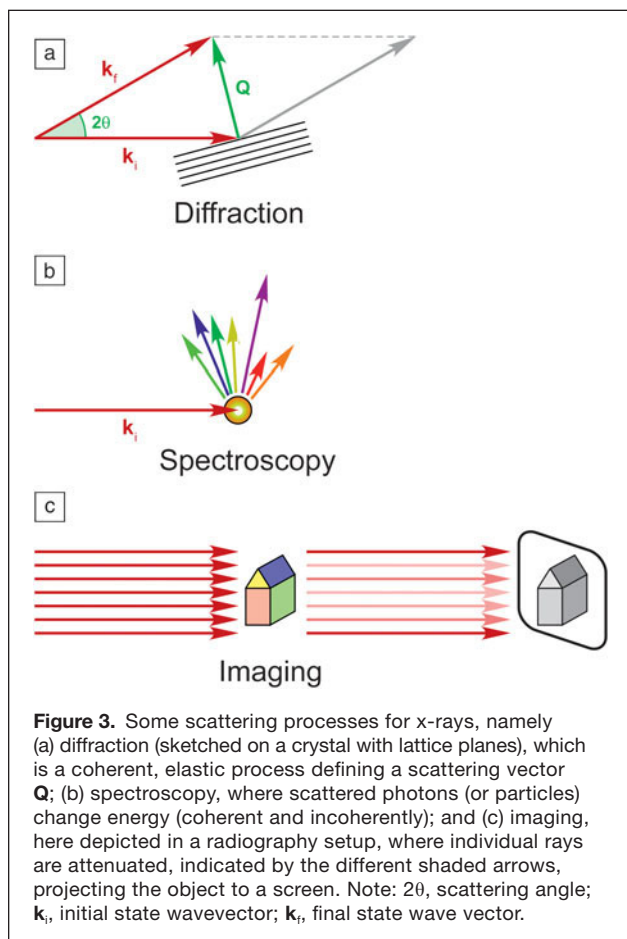
Within the scope of hard- and soft-matter sciences, x-rays interact with a specimen, and scattered primary or secondary radiation is detected in order to characterize the material. Based on the method of scattering and interaction with the specimen, one classification scheme divides the techniques into the categories of diffraction, spectroscopy, and imaging (**Figure 3**); however, these processes can overlap and integrate with each other.

Imaging, where an object is placed in a beam and an image is recorded through optical mapping, involving projection as

in radiography and in topography⁴ or transformation through an optical lens or element is the most intuitive technique. Numerous variations of these basic techniques exist using the lateral coherence of the x-ray beam for phase-contrast imaging, where in an extreme case, an interface or edge between two fully transparent media is mapped by its difference in refractive index. So-called Fresnel diffraction at the media edge is due to the beams slightly deviating from each side of the edges and overlapping in the distance, resulting in interference fringes and thus an image of the edge.⁵

Both spectroscopy and diffraction probe for scattered or secondary photons. In coherent scattering, an x-ray wave can be described by a space-, \mathbf{x} , and time-, t , dependent oscillatory function $\exp(i(\mathbf{k}\mathbf{x} - \omega t))$ of wave vector \mathbf{k} , wavenumber $k = |\mathbf{k}|$, and angular frequency ω . Both \mathbf{k} and ω can potentially change by $\mathbf{Q} = \Delta\mathbf{k} = \mathbf{k}_f - \mathbf{k}_i$ and $\Delta\omega = \omega_f - \omega_i$, where indices i and f denote initial and final states, respectively. Usually, the distinguishing feature for spectroscopy





is $\Delta\omega \neq 0$, with energy transfer as $\Delta E = \hbar\Delta\omega$, where \hbar is the reduced Planck constant. In contrast, diffractometry investigates the scattered waves as a function of scattering vector \mathbf{Q} , also called the wave vector transfer, and momentum transfer $\Delta\mathbf{p} = \hbar\Delta\mathbf{k}$.

For conventional x-ray diffraction in powders, single crystals, and amorphous substances, $\Delta\omega = 0$, in other words, elastic scattering occurs. In their article in this issue, Simons et al. describe how in modern methods, these regimes of diffraction, spectroscopy, and imaging can be combined and interwoven, such as diffraction-contrast imaging in topographic methods, and particularly in dark-field x-ray microscopy. Both spectroscopic and diffraction methods can be used to scan a sample in order to form a raster map or image, taking advantage of scattered or secondary photons, as applied in fluorescence spectroscopy and reported by Liu and Weng (see their article in this issue), or in white beam Laue microdiffraction, as discussed in the X. Chen et al. article.

In their article, Glazer et al. discuss the application of high-energy x-rays for the study of materials relevant to the realization of modern Li-ion batteries. Such materials are of worldwide interest, employing both synchrotron⁶ and neutron radiation⁷ on dedicated beamlines. Because of the availability of small and brilliant x-ray beams, small specimens can be

investigated in tiny volumes under extreme conditions, as reviewed by B. Chen et al. in their article on high-pressure studies. Experimental access to high-pressure (10–100 GPa) and temperature (cryogenic to 5000 K) extreme conditions allows not only for investigation of materials as they occur in the interior of the earth,^{8,9} but also for the synthesis of new materials and the study of their fundamental properties. Large-volume multi-anvil pressure cells for specimens of several cubic millimeters have become useful for materials scientists to study microstructure evolution and segregation chemistry during high-pressure thermomechanical processing of engineering-relevant materials,¹⁰ and are nowadays complemented by an apparatus allowing uniaxial stress components.¹¹

Applications of synchrotron x-rays in materials research

High-energy x-rays for bulk investigations

Many applications of high-energy x-rays have been developed over the past two decades, spreading into a multitude of disciplines. The main advantage of x-rays with energies above 80 keV is the high penetration into bulk materials, which can exceed one centimeter in steel.¹² In the 1970s, Freund and Schneider pioneered crystal defect studies using 412 keV x-rays obtained from a radioactive gold γ -ray source.¹³ This was followed by the first 145 keV synchrotron high-energy diffraction studies at the Cornell High Energy Synchrotron Source (CHESS),¹⁴ and subsequently, the high-energy synchrotron beamlines BW5 (and preceding temporary setup) at Hamburger Synchrotronstrahlungslabor at DESY¹⁵ and ID15 at ESRF.¹⁶ Early applications in materials science evolved from ultrahigh-resolution single-crystal studies,^{17,18} investigations of amorphous materials, and pair distribution function analysis,^{19,20} as well as studies on magnetism.^{21,22}

Further work by Reimers led to a breakthrough in engineering studies using the ESRF for strain–stress analysis by an energy-dispersive method.^{23,24} The potential for bulk texture analysis has also been demonstrated.²⁵ The introduction of two-dimensional (2D) detectors for high-energy x-rays has opened up capabilities for large-area reciprocal space mapping, such as for studies of diffuse scattering,²⁶ simultaneous recording of many 2D powder diffraction rings, so-called Debye–Scherrer rings,²⁷ leading to advanced texture analysis,²⁸ three-dimensional x-ray diffraction techniques²⁹ that map microstructures in volume, and the materials oscilloscope.^{30,31} In the latter, the intensity distribution of distinguishable diffraction spots, lying on the Debye–Scherrer rings and stemming from individual crystallites, is streaked along a time axis while the specimen undergoes thermomechanical processing, leading to characteristic traces or “timelines” that help to distinguish various deformation and annealing processes, such as grain coarsening, refinement, subgrain formation, rotation, slip, twinning, (dynamic) recovery, and recrystallization.

Modern applications of high-energy x-rays cover time-resolved *in situ* and *operando* experiments, such as the overview of energy-storage materials by Glazer et al. in their article.

They report on battery research, from the reaction and structural transformation during the synthesis of cathode materials; to structural changes in the first lithium loading cycle; and to investigations during the charging and discharging processes of an entire lithium battery. Because of the fine spot size of the x-ray beams today, together with their bulk penetration, studies of buried layers can be conducted, such as in different battery components.

Principles of two-dimensional x-ray diffraction

In conventional powder x-ray diffraction, intensity is recorded against a single dimension, for example, scattering angle 2θ . This diffraction involves rotational symmetry about the primary beam axis, leading to so-called Debye–Scherrer cones in space. In a typical experimental setup (Figure 4), bundled high-energy x-rays impinge onto a sample volume, while a 2D detector maps these cones to Debye–Scherrer rings at a given distance. The radial intensity distribution of those rings corresponds to a conventional x-ray diffractogram, where the radius is transformed into scattering angles 2θ , or even better, into $Q = 2k \sin(\theta) = 4\pi/\lambda \sin(\theta)$, where λ is the x-ray wavelength. In order to increase the intensity, Debye–Scherrer rings are azimuthally integrated if the pattern is isotropic. Such Q -dependent information not only allows extraction of phase changes, but also allows for obtaining microstrain and particle sizes from line broadening. The broadening contributions can be separated by their dependence on scattering transfer Q : since strain $\varepsilon = -\Delta Q/Q$, strain broadening increases linearly with Q , while size broadening transforms

into reciprocal space by a constant $\Delta Q \approx 2\pi/D$ for crystallites of coherent size D .

Most often, however, strain and particle size are crystallographically anisotropic and also exhibit some distribution, transforming the use of these basic relations into the use of more complicated fitting and modeling procedures.³²

Anisotropy may occur in uniaxially loaded specimens and in textured samples,³³ for which such 2D patterns can be sectored^{31,34} and evaluated along their orientation. In extreme cases, the azimuthal distribution of intensity along the rings is either continuous, stemming from a large number of randomly oriented grains, or shows only a few spots, if any, to be identified as a reflection from a single crystal or crystallite. A small number of reflecting crystallites results in a low number of spots on the rings, and their distribution has been traced by the previously mentioned materials oscilloscope, for instance in plastic-deformation processes at high temperatures (Figure 5).³¹ The spots are not intrinsically sharp, but are convolved with the beam size. Moreover, they map features of the reflecting grain, which may consist of subgrains with slightly different orientations and stress states.³⁵ Mapping of these spots has been developed by some groups,³⁶ and is now driven by the introduction of magnifying optics in the spot beam path, as described in the Simons et al. article.

Imaging and spatial mapping

X-ray topography,³⁷ called dark-field imaging in electron microscopy, is the mapping of a crystal reflection onto a 2D detector and resolving contrasts from various origins. The

latter can be crystal distortions, changes in the intensity by increasing the extinction depth, or small-angle grain boundaries by displacing parts of the diffracted beam under an angle such that their imprints can partly overlap or have a gap, resulting in a bright or a dark line, respectively. In parallel to electron backscatter diffraction, orientations of subgrains can be mapped and further evaluated, such as orientation boundaries, and peak width, as described in the Simons et al. article. Here, x-rays have the advantage of much higher intrinsic angular resolution as compared to electron diffraction and are capable of resolving local strain and derivative strain components in the examined material.

Another diffraction-mapping method presented by X. Chen et al. in their article is the application of white beam Laue diffraction as a function of position, as well as rastering the image. In contrast to monochromatic-beam diffraction, as previously explained, a white beam that contains a continuous spectrum impinges a crystal. Then, for a given reciprocal lattice vector length and orientation, a matching wave vector is selected from a large range of wave vectors. Thus, a reflection always exists

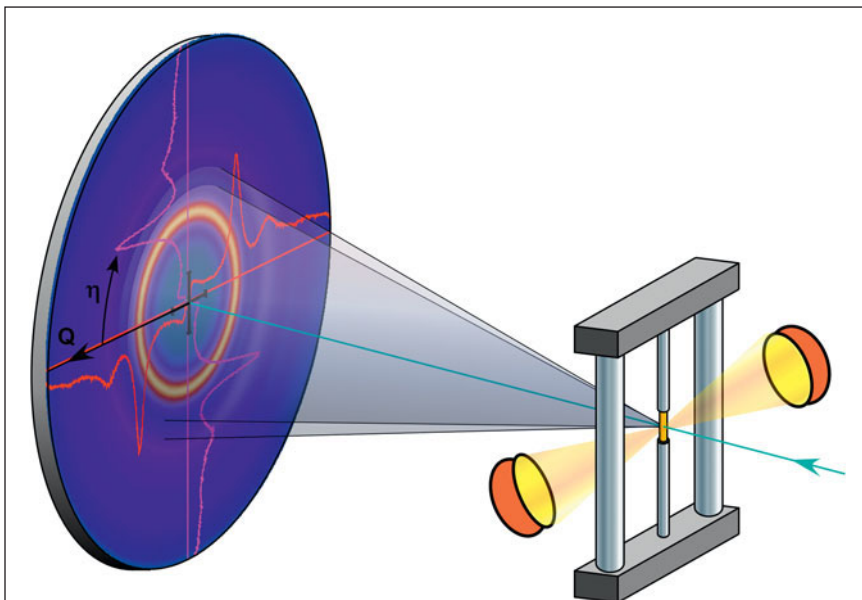
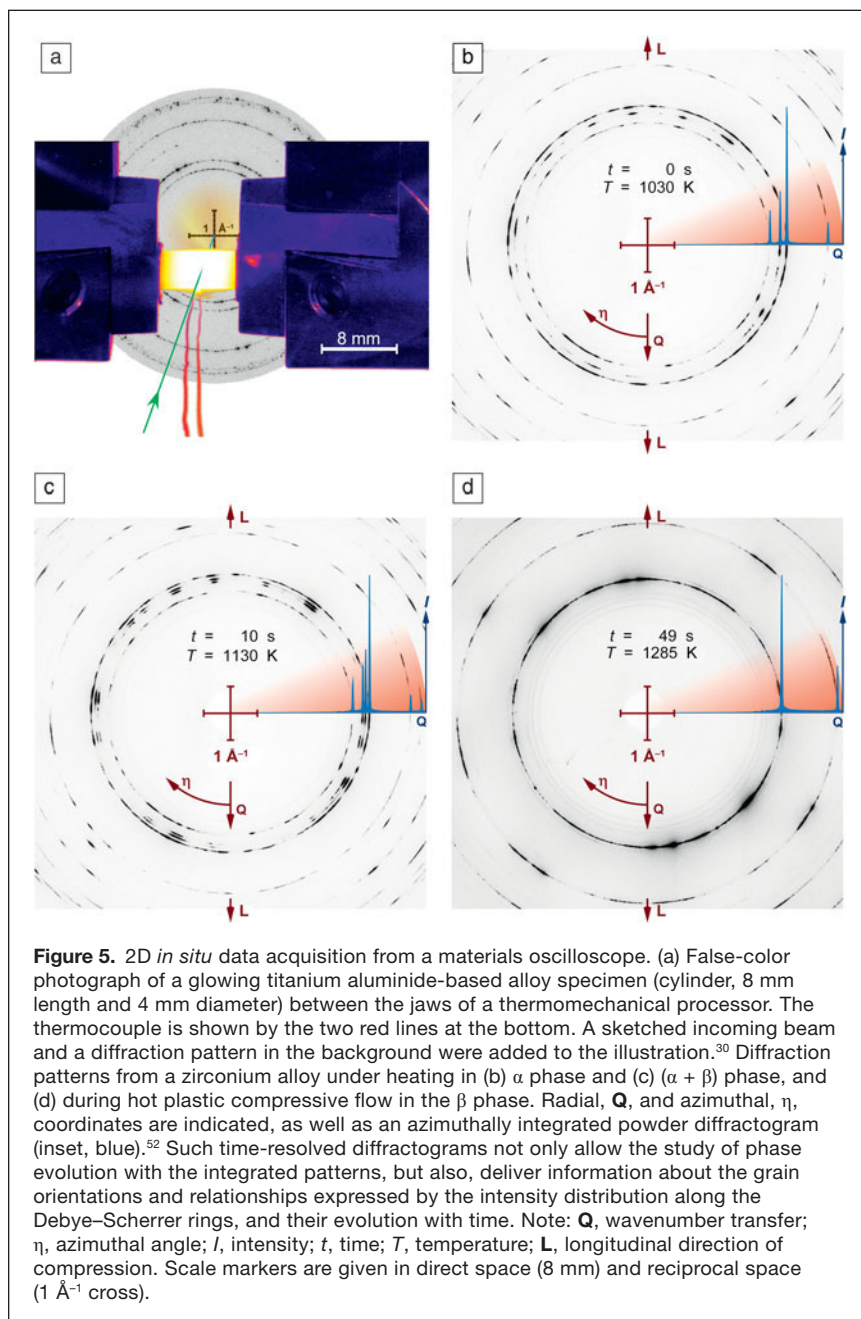


Figure 4. Typical 2D high-energy x-ray diffraction setup: a small beam arriving from the right is scattered by the specimen into Debye–Scherrer cones, which are mapped as diffraction rings on a flat-panel detector. Superimposed to the 2D detector image are four radial sections of the intensity, as further illustrated in Figure 5. The specimen is in a mechanical load frame, heated by halogen lamps; however, a vast variety of sample environments can be designed, such as an *in operando* battery cell, and reaction chambers. Note: Q , scattering vector; η , azimuthal angle.



for any arbitrary orientation, within the half space of Q oriented toward the incident beam and within the limits of the incident spectral distribution. For a single crystal, a multitude of reciprocal lattice vectors (i.e., lattice-plane orientations) results in a set of diffraction spots, from which the orientation of the crystal can be determined. Again, if lattice defects (e.g., dislocations and small-angle grain boundaries) exist, peaks spread out into streaks or distributions, respectively.^{38,39}

In particular, the white beam Laue method has been combined with micro- and nanometer-sized beam diffraction, resolving local structures, and key information has been collected in a book edited by two of the pioneers of this field, Barabash and Ice.⁴⁰

More generally, both white and monochromatic micro- and nanobeam diffraction methods have evolved in various fields of research. Besides the trend of extensive applications in geophysics,⁴¹ mineralogy, and biomineralogy,^{42,43} the intensive combination with electron microscopy to explore the nanoscale world^{44,45} has matured, in conjunction with ongoing improvements in the data-analysis approaches.^{46,47} The article by X. Chen et al. emphasizes some new features and further developments of these techniques, including the significant improvement of spatial resolution at the Taiwan Photon Source, and small-molecule structure refinement by interpreting the monochromatic and polychromatic x-ray diffraction signals from the same crystal.

Besides the discipline of diffraction, spectroscopic methods are widely established at synchrotron sources. In their article, Liu and Weng present an example of the soft x-ray range using absorption spectroscopy. Absorption based on the photoelectric effect is achieved when a bound electron, often inner K or L electrons, is excited by the x-rays, leaving a hole (**Figure 6**). In this process, the x-ray energy must be sufficient to overcome the binding potential energy of the electron sitting in the atomic shell. When the x-ray energy is scanned upward, higher absorption occurs suddenly in a step pattern at the edge, where the threshold is overcome and the photon energy becomes sufficient to eject the electron. Since, in principle, that same electron could fill the hole again, which is stimulated light emission, the entire process is a coherent resonance phenomenon, where the wave function of the simultaneously bound and freed electron needs to be considered in detail, including its extension to its nearest neighbors.

As the electron wave backscatters toward the hole, the stimulated emission contribution, and thus the whole absorption process, varies in amplitude and yields observable fringes in the absorption spectrum. The electron-wave interference pattern depends sensitively on both electron wavelength (which changes with the x-ray energy) and the local morphology of the electron cloud where the atom sits (i.e., its local crystal structure or other environment), leading to the extended x-ray absorption fine structure, known as EXAFS. In particular, the oxidation state of an ion defines the local environment, namely at the absorbing atom itself, leading to fingerprint-like characteristics at or close to the edge, allowing determination of the oxidation state. The energy of the absorption

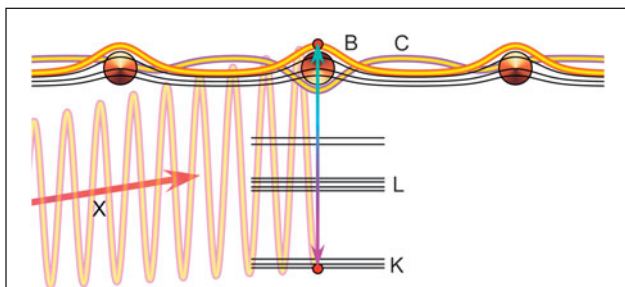


Figure 6. Schematic for the formation of an x-ray absorption fine structure. Absorption takes place by ejecting a core electron of the central atom from the K or L shell into the conduction band B or C, where it can travel to neighboring atoms and scatter back. The electron amplitude and energy levels depend minutely on the interference of these traveling waves, which depend on energy. Here, band state B has a slightly higher energy level than band state C at the central atom. The scattering process is a superposition of the absorption and stimulated emission of light, and lasts on a femtosecond scale. This process involves many attosecond cycles of the x-ray wave (X), during which a standing electron wave builds up, thus modulating the absorption probability. In quantum mechanics, the process of absorption is not localized at a fixed position, but instead is distributed over many equivalent atoms, giving rise to the interference.

edges is dictated by the nature of the atoms, covering the very soft and soft x-rays for the lighter elements, hard x-rays for the K-edges of medium elements, and L-edges of heavier elements.⁴⁸

The details and variations of absorption spectroscopy are more deeply explored in Liu and Weng's article. They present example applications and a study that further explores the chemical bonds at the solid–electrolyte interface in Li-ion batteries, making a thematic link to the diffraction work by Glazer et al. Similarly, the B. Chen et al. article reports on the complementary nature of absorption spectroscopy and diffraction as well as the characterization of materials under high pressure.

Conclusion

Advanced synchrotron-based techniques, especially for materials research, have continuously emerged and evolved in the past decades. A number of facilities and beamlines are currently being created, upgraded, and refurbished around the world. On the basis of the knowledge and experience gained in the first 10–20 years of large third-generation sources, new, dedicated beamlines are being installed for specific purposes, such as battery research,⁶ by commercial companies.⁴⁹ These beamlines, for example, the Hard X-Ray Nanoprobe Facility at the National Synchrotron Light Source II at Brookhaven National Laboratory, are also combining a multitude of different scattering, diffraction, and imaging techniques.⁵⁰

At the same time, synchrotron sources, including free-electron lasers, have also been upgraded to perform at their extremes, delivering diffraction-limited, coherent beams and ultrashort time scales. Specific sample environments, such as high-pressure apparatus, chemical reactors, and thermomechanical processors have been developed and are complemented

by automated, smart, and comprehensive computing power and algorithms for data analysis.

Synchrotron radiation is not the only modern probe for which highly sophisticated facilities are needed. Future research trends in applications will have to utilize their complementarity, such as neutron and synchrotron radiation for structural studies, neutrons and muons for magnetism studies, light scattering, synchrotrons, and neutrons for the study of the dynamics of the materials, positrons, and synchrotron x-rays for the measurement of electronic density of states, ions and diffraction for the study of crystal defects, and electrons, x-rays, and neutrons for texture analysis. Such quantum-beam science is currently led by centers and organizations operating at least two or more such facilities and user groups. In addition, they have created a dedicated journal.⁵¹ With this potential, we are looking forward to an even brighter future for this field.

Acknowledgments

K.C. is supported by the National Young 1000 Talents Program of China, the National Natural Science Foundation of China (Grant No. 51302207), the National Basic Research Program of China (“973” Program) (Grant No. 2015CB057400), the Collaborative Innovation Center of High-End Manufacturing Equipment, and the International Joint Laboratory for Micro/Nano Manufacturing and Measurement Technologies.

References

1. C. Kunz, M. Skibowski, B. Sonntag, *Synchrotron Radiat. News* **28**, 16 (2015).
2. K.-D. Liss, A. Bartels, A. Schreyer, H. Clemens, *Textures Microstruct.* **35**, 219 (2003).
3. S. Ribeiro, S. Okada, <http://www.lightsources.org>.
4. J. Baruchel, P. Bleuet, A. Bravin, P. Coan, E. Lima, A. Madsen, W. Ludwig, P. Pernot, and J. Susini, *C. R. Phys.* **9**, 624 (2008).
5. S.W. Wilkins, T.E. Gureyev, D. Gao, A. Pogany, A.W. Stevenson, *Nature* **384**, 335 (1996).
6. H. Tanida, K. Fukuda, H. Murayama, Y. Orikasa, H. Arai, Y. Uchimoto, E. Matsubara, T. Uruga, K. Takeshita, S. Takahashi, M. Sano, H. Aoyagi, A. Watanabe, N. Nariyama, H. Ohashi, H. Yumoto, T. Koyama, Y. Senba, T. Takeuchi, Y. Furukawa, T. Ohata, T. Matsushita, Y. Ishizawa, T. Kudo, H. Kimura, H. Yamazaki, T. Tanaka, T. Bizen, T. Seike, S. Goto, H. Ohno, M. Takata, H. Kitamura, T. Ishikawa, T. Ohta, Z. Ogumi, *J. Synchrotron Radiat.* **21**, 268 (2014).
7. M. Yonemura, K. Mori, T. Kamiyama, T. Fukunaga, S. Torii, M. Nagao, Y. Ishikawa, Y. Onodera, D.S. Adipranoto, H. Arai, Y. Uchimoto, Z. Ogumi, *J. Phys. Conf. Ser.* **502**, 012053 (2014).
8. R.J. Hemley, H.-K. Mao, *Int. Geol. Rev.* **43**, 1 (2001).
9. W.L. Mao, H.K. Mao, J. Shu, Y. Fei, R.J. Hemley, Y. Meng, G. Shen, V.B. Prakapenka, A.J. Campbell, D.L. Heinz, W. Sturhahn, J. Zhao, *Geochim. Cosmochim. Acta* **70**, A389 (2006).
10. K.-D. Liss, K. Funakoshi, R.J. Dippenaar, Y. Higo, A. Shiro, M. Reid, H. Suzuki, T. Shobu, K. Akita, *Metals* (forthcoming).
11. A. Sano-Furukawa, T. Hattori, H. Arima, A. Yamada, S. Tabata, M. Kondo, A. Nakamura, H. Kagi, T. Yagi, *Rev. Sci. Instrum.* **85**, 113905 (2014).
12. A. Steuwer, J.R. Santisteban, M. Turski, P.J. Withers, T. Buslaps, *Nucl. Instrum. Methods Phys. Res. B* **238**, 200 (2005).
13. A. Freund, J. Schneider, *J. Cryst. Growth* **13–14**, 247 (1972).
14. J.B. Hastings, D.P. Siddons, L.E. Berman, J.R. Schneider, *Rev. Sci. Instrum.* **60**, 2398 (1989).
15. H.F. Poulsen, S. Garbe, T. Lorentzen, D. Juul Jensen, F.W. Poulsen, N.H. Andersen, T. Frello, R. Feidenhansl, H. Graafsma, *J. Synchrotron Radiat.* **4**, 147 (1997).
16. P. Suortti, T. Tschentscher, *Rev. Sci. Instrum.* **66**, 1798 (1995).
17. R. Bouchard, D. Hupfeld, T. Lippmann, J. Neuefeind, H.B. Neumann, H.F. Poulsen, U. Rütt, T. Schmidt, J.R. Schneider, J. Süßenbach, M. von Zimmermann, *J. Synchrotron Radiat.* **5**, 90 (1998).

18. K.D. Liss, A. Royer, T. Tschentscher, P. Suortti, A.P. Williams, *J. Synchrotron Radiat.* **5**, 82 (1998).
19. J. Neufeind, K.D. Liss, *Ber. Bunsenges. Phys. Chem.* **100**, 1341 (1996).
20. T. Egami, S.J.L. Billinge, *Underneath the Bragg Peaks: Structural Analysis of Complex Materials* (Elsevier, Sydney, 2003).
21. J. Strempler, T. Bruckel, T. Rutt, J.R. Schneider, K.D. Liss, T. Tschentscher, *Acta Crystallogr. A* **52**, 438 (1996).
22. T. Chattopadhyay, K.D. Liss, T. Bruckel, *J. Magn. Magn. Mater.* **177**, 1058 (1998).
23. W. Reimers, M. Broda, G. Bruschi, D. Dantz, K.D. Liss, A. Pyzalla, T. Schmackers, T. Tschentscher, *J. Nondestruct. Eval.* **17**, 129 (1998).
24. W. Reimers, A. Pyzalla, M. Broda, G. Bruschi, D. Dantz, T. Schmackers, K.D. Liss, T. Tschentscher, *J. Mater. Sci. Lett.* **18**, 581 (1999).
25. H.J. Bunge, L. Wcislak, H. Klein, U. Garbe, J.R. Schneider, *Adv. Eng. Mater.* **4**, 300 (2002).
26. T.R. Welberry, *Rep. Prog. Phys.* **48**, 1543 (1985).
27. E.M. Lauridsen, D.J. Jensen, H.F. Poulsen, U. Lienert, *Scr. Mater.* **43**, 561 (2000).
28. L. Lutterotti, M. Bortolotti, G. Ischia, I. Lonardelli, H.-R. Wenk, *Z. Kristallogr.* **26**, Suppl. 125 (2007).
29. H.F. Poulsen, S.F. Nielsen, E.M. Lauridsen, S. Schmidt, R.M. Suter, U. Lienert, L. Margulies, T. Lorentzen, D. Juul Jensen, *J. Appl. Crystallogr.* **34**, 751 (2001).
30. K.-D. Liss, *Proc. ICCE-23* **457**, 1 (2015).
31. K.-D. Liss, K. Yan, *Mater. Sci. Eng. A* **528**, 11 (2010).
32. T. Ungár, J. Gubicza, G. Ribárik, A. Borbély, *J. Appl. Crystallogr.* **34**, 298 (2001).
33. U.F. Kocks, C.N. Tomé, H.-R. Wenk, *Texture and Anisotropy: Preferred Orientations in Polycrystals and Their Effect on Materials Properties* (Cambridge University Press, Cambridge, 2000).
34. K.-D. Liss, D. Qu, K. Yan, M. Reid, *Adv. Eng. Mater.* **15**, 347 (2013).
35. K.-D. Liss, A. Bartels, H. Clemens, S. Bystrzanowski, A. Stark, T. Buslaps, F.-P. Schimansky, R. Gerling, C. Scheu, A. Schreyer, *Acta Mater.* **54**, 3721 (2006).
36. U. Lienert, S.F. Li, C.M. Hefferan, J. Lind, R.M. Suter, J.V. Bernier, N.R. Barton, M.C. Brandes, M.J. Mills, M.P. Miller, B. Jakobsen, W. Pantleon, *JOM* **63**, 70 (2011).
37. D.R. Black, G.G. Long, *X-Ray Topography* (Special Publication 960–10, National Institute of Standards and Technology, April 2004), http://www.nist.gov/manuscript-publication-search.cfm?pub_id=901559&division=852.
38. R. Barabash, G.E. Ice, B.C. Larson, G.M. Pharr, K.-S. Chung, W. Yang, *Appl. Phys. Lett.* **79**, 749 (2001).
39. R.I. Barabash, G.E. Ice, N. Tamura, B.C. Valek, J.C. Bravman, R. Spolenak, J.R. Patel, *J. Appl. Phys.* **93**, 5701 (2003).
40. R. Barabash, G. Ice, Eds., *Strain and Dislocation Gradients from Diffraction: Spatially-Resolved Local Structure and Defects* (Imperial College Press, 2014).
41. K. Chen, M. Kunz, N. Tamura, H.-R. Wenk, *Geology* **43**, 219 (2015).
42. T. Zhang, Y. Ma, K. Chen, M. Kunz, N. Tamura, M. Qiang, J. Xu, L. Qi, *Angew. Chem. Int. Ed.* **50**, 10361 (2011).
43. N. Tamura, P.U.P.A. Gilbert, in *Methods in Enzymology*, Research Methods in Biomineralization Science Series, J.J. De Yoreo, Ed. (Academic Press, 2013), pp. 501–531.
44. Q. Yu, L. Qi, K. Chen, R.K. Mishra, J. Li, A.M. Minor, *Nano Lett.* **12**, 887 (2012).
45. H. Guo, K. Chen, Y. Oh, K. Wang, C. Dejoie, S.A. Syed Asif, O.L. Warren, Z.W. Shan, J. Wu, A.M. Minor, *Nano Lett.* **11**, 3207 (2011).
46. K. Chen, C. Dejoie, H.-R. Wenk, *J. Appl. Crystallogr.* **45**, 982 (2012).
47. Y. Li, L. Wan, K. Chen, *J. Appl. Crystallogr.* **48**, 747 (2015).
48. A. Thompson, I. Lindau, D. Attwood, Y. Liu, E. Gullikson, P. Pianetta, M. Howells, A. Robinson, K.-J. Kim, J. Scofield, J. Underwood, J. Kortright, G. Williams, H. Winick, *X-Ray Data Booklet*, 3rd ed. (LBNLPUB-490 Lawrence Berkeley National Laboratory, Berkeley, CA, 2009).
49. Y. Hirose, in *SPRING-8 Research Frontiers 2009* (SPRING-8, 2010), p. 170.
50. Y. Chu, H. Yan, E. Nazaretski, S. Kalbfleisch, X. Huang, K. Lauer, N. Bouet, "Hard X-Ray Nanoprobe Facility at the National Synchrotron Light Source II," *SPIE Newsroom*, published online August 31, 2015, available at <http://dx.doi.org/10.1117/2.1201508.006068>.
51. M. Rittman, K.-D. Liss, Eds., *Quantum Beam Science—An Open Access Journal from MDPI* (MDPI, Basel, Switzerland, 2016), <http://www.mdpi.com/journal/qubs>.
52. K.-D. Liss, *World J. Eng.* **7** (S2), P438 (2010). □



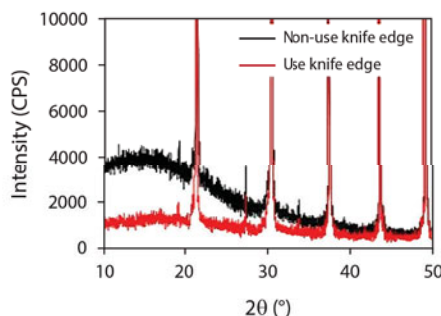
XRD WITH VARIABLE KNIFE EDGE FEATURE



Rigaku MiniFlex300/600 can be equipped with the D/teX Ultra high-speed 1-dimensional detector to obtain greater intensity. This detector has a broad detection surface and can efficiently count diffraction X-rays from a sample. As a result, it is possible to obtain intensities from a few tens to roughly 100 times greater than a scintillation counter. Background can also be reduced using the fluorescent X-ray reduction mode or the knife edge feature. The figure shows the X-ray diffraction patterns obtained when a knife edge is installed versus no knife edge. By using a knife edge, it is possible to achieve an extreme reduction in scattering on the low-angle side. Also, the knife edge moves in a way which is dependent on the diffraction angle 2θ , and thus there is no blind spot (intensity attenuation) on the high-angle side, and measurement can be done from the low-angle side to the high-angle side.

MiniFlex

X-ray diffraction patterns (enlarged) of zeolite, measured when a knife edge is installed versus no knife edge.



APP
BYTE

Rigaku Corporation and its Global Subsidiaries
www.Rigaku.com | info@Rigaku.com